Supporting Information

Scissor g-C$_3$N$_4$ for high-density loading of catalyst domains in mesoporous thin-layer conductive network for durable Li-S batteries

Chuanzhong Lai[1,2,3,#], Xuejun Zhou[1,3,#], Meng Lei[1,3], Wenlong Liu[1,2,3], Xiaoke Mu[4], Chilin Li[1,2,3]

[1]State Key Laboratory of High Performance Ceramics and Superfine Microstructure, Shanghai Institute of Ceramics, Chinese Academy of Sciences, Shanghai 201899, China.

[2]Center of Materials Science and Optoelectronics Engineering, University of Chinese Academy of Sciences, Beijing 100049, China.

[3]CAS Key Laboratory of Materials for Energy Conversion, Shanghai Institute of Ceramics, Chinese Academy of Sciences, Shanghai 201899, China.

[4]Institute of Nanotechnology (INT), Karlsruhe Institute of Technology, Eggenstein-Leopoldshafen 76344, Germany.

[#]Authors contributed equally.

Correspondence to: Prof. Chilin Li, State Key Laboratory of High Performance Ceramics and Superfine Microstructure, Shanghai Institute of Ceramics, Chinese Academy of Sciences, 585 He Shuo Road, Shanghai 201899, China. E-mail: chilinli@mail.sic.ac.cn
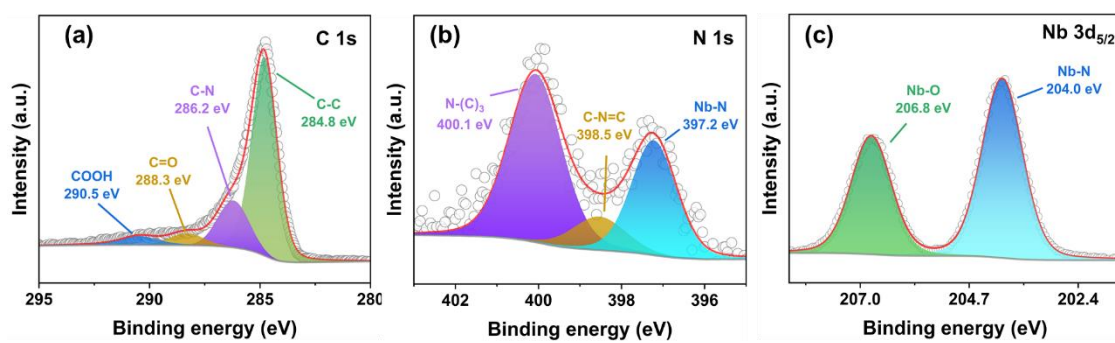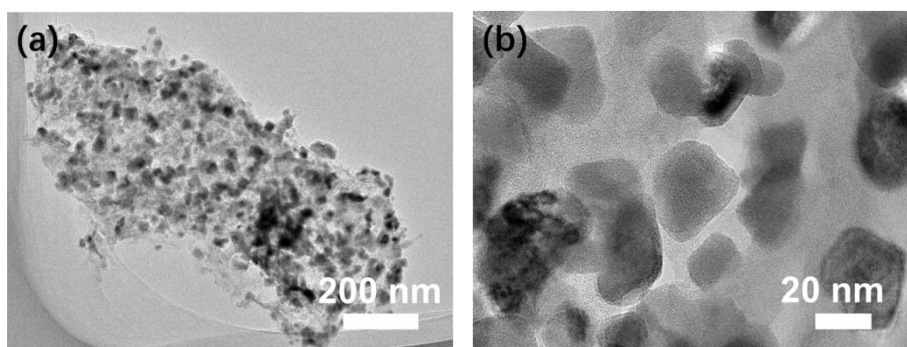
Figure S1. XPS results of as-synthesized NbN/C powder: (a) C 1s, (b) N 1s, (c) Nb $3d_{5/2}$.
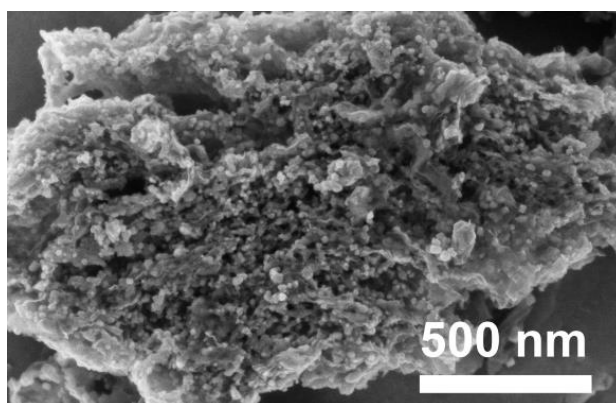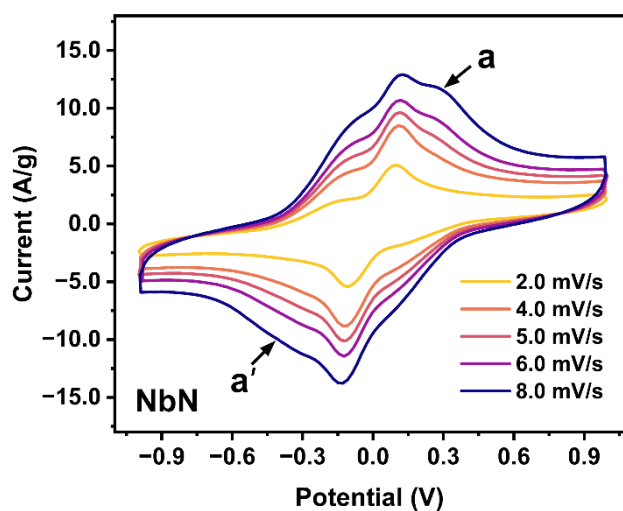

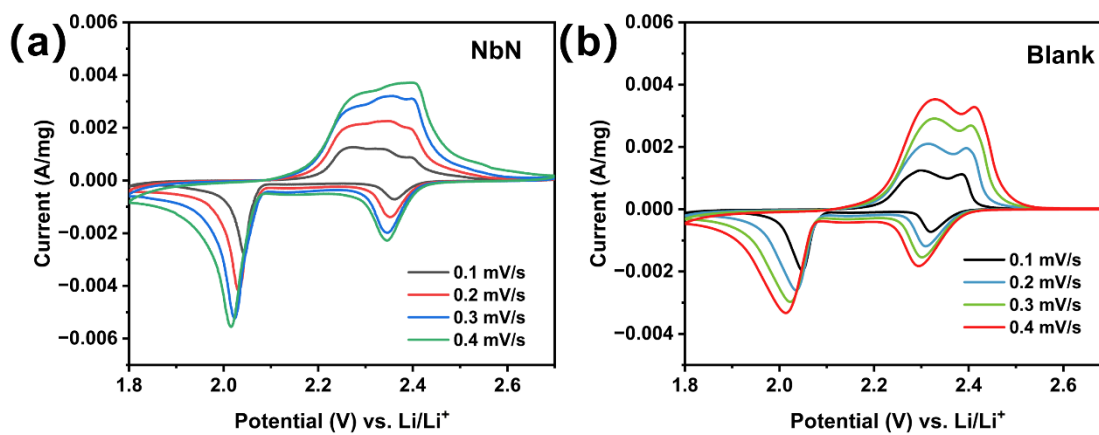**Figure S2**. SEM image of as-synthesized NbN/C powder.
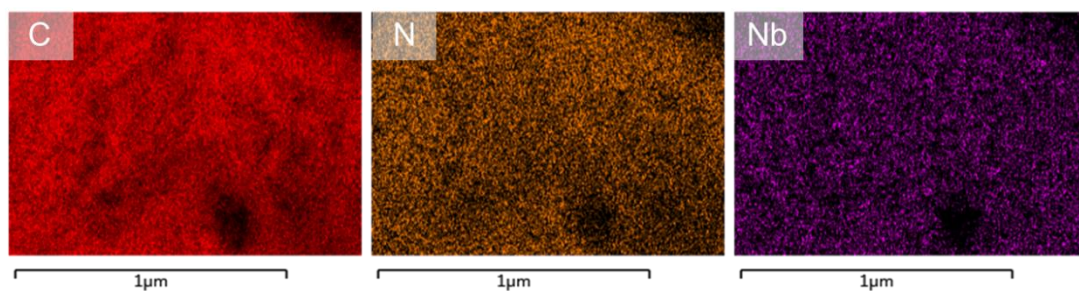
Figure S3. EDS mapping of as-synthesized NbN/C powder.

Figure S4. TEM images of as-synthesized NbN/C powder in different scales.

Figure S5. CV test on the symmetric Li|Li cell with the NbN/C@PP separator at different scan rates from 2.0 to 8.0 mV s^{-1}.

Figure S6. CV tests on the Li-S cells based on different separators of (a) NbN/C@PP and (b) pristine PP at different scan rates from 0.1 to 0.4 mV s^{-1}.
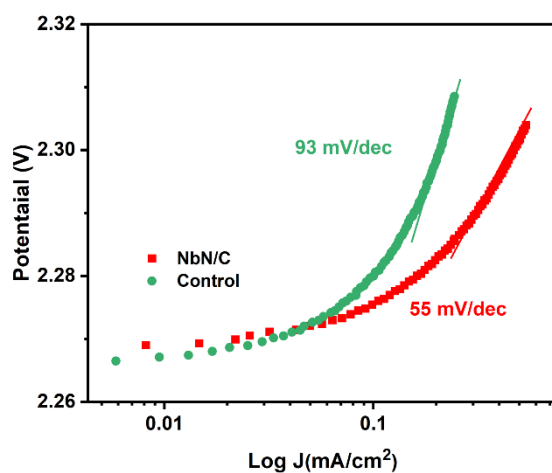
Figure S7. Tafel plots of the Li-S cells based on different separators corresponding to the oxidation stage from Li_2S_n to sulfur.
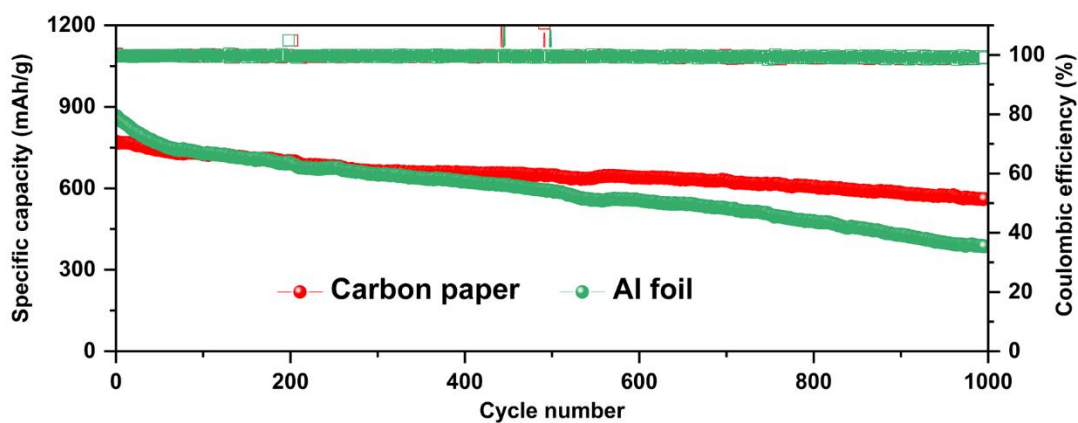
Figure S8. Electrochemical performance of Li-S cells with different current collectors under a rate of 2 C.

Figure S9. Electrochemical performance of Li-S cells with different high S-mass loading cathodes.
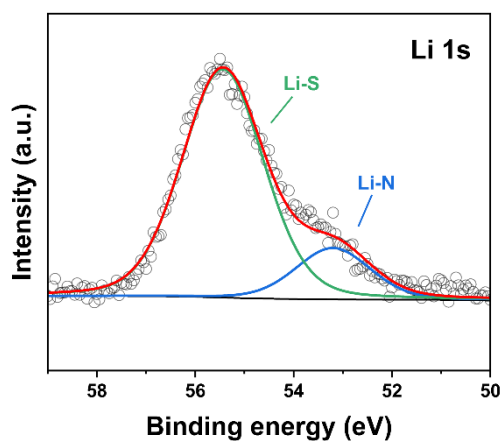
Figure S10. XPS result of Li 1s for the cycled NbN/C@PP separator.

Table S1. Comparison of adsorption energies of LiPSs on the surfaces of different materials.

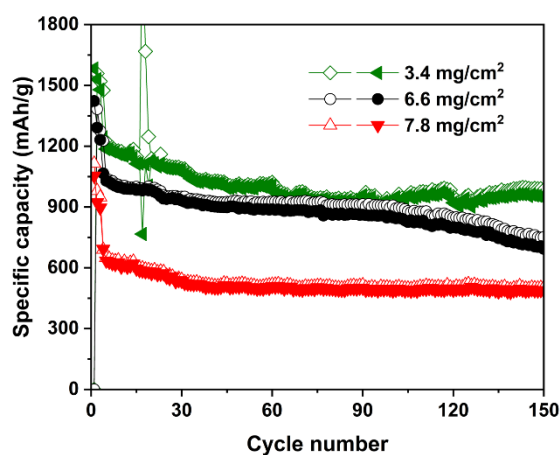| Materials	Adsorption energy (eV)						Reference
	Li_2S	Li_2S_2	Li_2S_4	Li_2S_6	Li_2S_8	S_8	
NbC (001)	—	—	—	-2.91	—	—	Ref. S1
NiO (111)	—	—	-2.39	-2.36	-3.14	—	Ref. S2
NbN (111)	—	—	-5.21	-2.74	-4.63	—	Ref. S3
NbN (200)	—	—	-3.54	—	—	—	Ref. S4
VN (200)	-3.86	-3.14	-3.27	-3.01	-3.46	-2.21	Ref. S5
NbN (200)	**-3.07**	**-3.04**	**-2.09**	**-2.53**	**-3.12**	**-2.04**	**This work**

Table S2. Energy barriers at different stages of conversion reactions based on various LiPSs obtained from the calculated Gibbs free energies.

Conversion step	$S_8 \rightarrow Li_2S_8$	$Li_2S_8 \rightarrow Li_2S_6$	$Li_2S_6 \rightarrow Li_2S_4$	$Li_2S_4 \rightarrow Li_2S_2$	$Li_2S_2 \rightarrow Li_2S$
Energy barrier (eV)	-3.42	0.53	0.7	0.39	0.81

Table S3. Mass fractions of cell components and E/S ratio, N/P capacity ratio.

	Mass fraction of battery component					E/S ratio (μL/mg)	N/P capacity ratio
Battery container	NbN/C@PP	Lithium anode	S cathode	Electrolyte			
2.53 g	0.00635 g	0.0188 g	0.00522 g	0.034 g		—	—
97.3%	0.244%	0.723%	0.201%	1.31%		5	8.31

Table S4. The performance comparison of high loading sulfur batteries.

S loading (mg/cm²)	E/S ratio (μL/mg)	Current density (1 C = 1672 mA/g)	Cycle number	Capacity retention (mAh/g)	Reference
7.6	5.0	0.05 C	40	605.3	Ref. S6
4.06	5.0	1 C	500	340.4	Ref. S7
5.6	10	0.1 C	30	732.1	Ref. S8
5.3	9.43	0.1 C	45	754.7	Ref. S9
5.8	4.0	0.1 C	55	730	Ref. S10
5.4		0.2 C	80	703.7	Ref. S11
5.8	5.2	0.2 C	100	775.9	Ref. S12
6.6	7.0	0.2 C	100	686.2	Ref. S13
6.6	**5.0**	**1 mA/cm² (~ 0.1 C)**	**100**	**850**	**This work**

Note S1. Detailed information on how to get the activation energy difference for modified and control cells based on the Tafel plots.

According to the CV tests in Figure 4a under a scan rate of 0.2 mV s⁻¹, the relationship between electrode potential and activation energy for the NbN/C modified or blank PP based cell can be calculated according to the equation:

$$E_a = E_a^0 + \alpha ZF\varphi_{cathode}(O_X/Red)_{IR} \qquad (1)$$

where E_a is the activation energy of reduction process, E_a^0 is the intrinsic activation energy, α is the symmetry coefficient, Z is the number of charge transfer, F is the

Faraday's constant, and $\varphi_{cathode}(O_X/Red)_{IR}$ is the irreversible potential during cycling.

According to the simplified Tafel equation:

$$\eta_{cathode} = a + b ln j_{cathode} \qquad (2)$$

where $\eta_{cathode}$ is the overpotential of cathode and $j_{cathode}$ is the current density of cathode, a and b are the factors that are determined according to the specific system. Here $b = -\frac{RT}{\alpha ZF}$ is obtained from the slope of Tafel curve in Figure 4d, 4e and S5.

Putting b into the Equation (1), a new equation can be obtained as follows:

$$E_a = E_a^0 - \frac{RT}{b}\varphi_{cathode}(O_X/Red)_{IR} \qquad (3)$$

Hence, the difference on the activation energies of the reductions from S$_8$ to Li$_2$S$_n$ (denoted as E_{a1} and E_{a1}') and from Li$_2$S$_n$ to Li$_2$S (denoted as E_{a2} and E_{a2}') for the modified and control cells are:

$$\Delta E_{a1} = E_{a1} - E_{a1}' = -8.63 \ kJ \ mol^{-1}$$
$$\Delta E_{a2} = E_{a2} - E_{a2}' = -19.08 \ kJ \ mol^{-1}$$

REFERENCES

S1. Huang Q, Chen M, Su Z, Tian L, Zhang Y, Long D. Rational cooperativity of nanospace confinement and rapid catalysis via hollow carbon nanospheres@ Nb-based inorganics for high-rate Li-S batteries. *Chem Eng J* 2021; 411: 128504. DOI: 10.1016/j.cej.2021.128504.

S2. Pu J, Wang T, Zhu X, et al. Multifunctional Ni/NiO heterostructure nanoparticles doped carbon nanorods modified separator for enhancing Li-S battery performance. *Electrochim Acta* 2022; 435: 141396. DOI: 10.1016/j.electacta.2022.141396.

S3. Qiu W, An C, Yan Y, et al. Suppressed polysulfide shuttling and improved Li$^+$ transport in Li-S batteries enabled by NbN modified PP separator. *J Power Sources* 2019; 423: 98-105. DOI: 10.1016/j.jpowsour.2019.03.070.

S4. Fan S, Huang S, Pam M E, et al. Design multifunctional catalytic interface: toward regulation of polysulfide and Li_2S redox conversion in Li-S batteries. *Small* 2019, 15: 1906132. DOI: 10.1002/smll.201906132.

S5. Ma L, Yuan H, Zhang W, et al. Porous-shell vanadium nitride nanobubbles with ultrahigh areal sulfur loading for high-capacity and long-life lithium-sulfur batteries. *Nano Lett* 2017; 17: 7839-7846. DOI: 10.1021/acs.nanolett.7b04084.

S6. Wu Q, Yao Z, Zhou X, Xu J, Cao F, Li C. Built-in catalysis in confined nanoreactors for high-loading Li-S batteries. *ACS Nano* 2020; 14: 3365-77. DOI: 10.1021/acsnano.9b09231.

S7. Feng J, Li J, Zhang H, et al. Accelerating redox kinetics by ZIF-67 derived amorphous cobalt phosphide electrocatalyst for high-performance lithium-sulfur batteries. *Energy Mater* 2023; 3: 300001. DOI: 10.20517/energymater.2022.62.

S8. Ye Z, Jiang Y, Li L, Wu F, Chen R. A high-efficiency CoSe electrocatalyst with hierarchical porous polyhedron nanoarchitecture for accelerating polysulfides conversion in Li-S batteries. *Adv Mater* 2020; 32: 2002168. DOI: 10.1002/adma.202002168.

S9. Shi Z, Sun Z, Cai J, et al. Boosting dual-directional polysulfide electrocatalysis via bimetallic alloying for printable Li-S batteries. *Adv Funct Mater* 2021; 31: 2006798. DOI: 10.1002/adfm.202006798.

S10. Ren Y, Zhai Q, Wang B, et al. Synergistic adsorption-electrocatalysis of 2D/2D heterostructure toward high performance Li-S batteries. *Chem Eng J* 2022; 439: 135535. DOI: 10.1016/j.cej.2022.135535.

S11. Shi M, Liu Z, Zhang S, et al. A Mott-Schottky heterogeneous layer for Li-S batteries: enabling both high stability and commercial-sulfur utilization. *Adv Energy Mater* 2022; 12: 2103657. DOI: 10.1002/aenm.202103657.

S12. Zhao Q, Wang R, Wen J, et al. Separator engineering toward practical Li-S batteries: targeted electrocatalytic sulfur conversion, lithium plating regulation, and thermal tolerance. *Nano Energy* 2022; 95: 106982. DOI: 10.1016/j.nanoen.2022.106982.

S13. Wang Y, Zhu L, Wang J, Zhang Z, Yu J, Yang Z. Enhanced chemisorption and catalytic conversion of polysulfides via CoFe@NC nanocubes modified separator for superior Li-S batteries. *Chem Eng J* 2022; 433: 133792. DOI: 10.1016/j.cej.2021.133792.